Article

Ligand Tuning in Cu(pyalk)₂ Water Oxidation Electrocatalysis

Claire C. Cody [ID], Zofia N. Caes, Matt D. Capobianco, Brandon Q. Mercado, Robert H. Crabtree and Gary W. Brudvig *[ID]

Department of Chemistry, Yale Energy Sciences Institute, Yale University, New Haven, CT 06520-8107, USA; claire.cody@yale.edu (C.C.C.)
* Correspondence: gary.brudvig@yale.edu

Abstract: Molecular copper water oxidation electrocatalysts have been extensively studied in recent years for their potential use in artificial photosynthetic systems for solar energy conversion. Although ligand modification and its ability to influence catalytic properties is a key advantage of molecular systems, there are, as yet, few examples of systematic studies of these effects. Our oxidatively resistant pyalk (2-pyridyl-2-propanoate) ligand forms a complex with copper(II) that catalyzes water oxidation and provides an attractive scaffold for systematic ligand tuning. Here, we report a series of analogous copper complexes with electron-donating (methoxy-) and -withdrawing (methoxycarbonyl-) groups at the para-position of the pyalk ligand. Trends in the pK_a and redox potential align with first-principles predictions for the electron-withdrawing and electron-donating groups. While the modified complexes show good activity for water oxidation, lowered faradaic efficiency in comparison to the parent complex highlights the importance of stability considerations for catalyst tuning.

Keywords: electrocatalysis; copper; ligand tuning; electron-withdrawing; electron-donating; cyclic voltammetry; water oxidation

1. Introduction

A promising avenue by which to address the storage challenge for wide-scale renewable energy implementation is to use solar energy to split water into oxygen and a chemical fuel such as hydrogen [1]. The rate-limiting step of this proposed photoelectrochemical system is water oxidation ($2H_2O \rightarrow O_2 + 4H^+ + 4e^-$), a thermodynamically and kinetically challenging reaction. Although well studied over the past few decades, water oxidation (WO) remains a bottleneck in these systems. Molecular water oxidation catalysts (WOCs) enable tunability, mechanistic understanding, and high turnover frequencies, providing insight for the rational development of highly efficient WOCs [2,3]. While ligand tuning is a key advantage of molecular systems, there remain few examples of systematic studies of the influence of ligand modification, especially for catalysts based on first-row transition metals.

Over the past several years, copper has attracted significant attention in the field of electrocatalytic WO for its well-defined coordination environment, biological relevance, and earth abundance relative to Ru- and Ir-based WOCs. Since the report of the first Cu-based WO electrocatalyst in 2012 [4], a number of Cu WOCs bearing mostly pyridine- and amine-based ligands have entered the literature, summarized well in a review by Sun and coworkers [5]. Recent reports include a trinuclear Cu complex with the highest reported turnover frequency for a Cu electrocatalyst by Chen et al. [6], and a Cu WOC based on a low-cost EDTA ligand from Yu et al. [7]. An important consideration for Cu WOCs is stability: under aqueous conditions and at relevant pH values, labile first-row metals can lose their ligands to form oxides and hydroxides [8,9]. It is, therefore, of interest to continue building our understanding of the factors governing catalytic activity and stability for Cu-based WOCs.

A common approach to investigating the mechanisms and ligand effects of homogeneous catalysts is to tune the electron density at the metal center by introducing electron-withdrawing or -donating substituents to the ligand backbone. Investigations of this type for Ru WOCs [10–13] have generally revealed trends of higher activity but lower stability for complexes bearing electron-donating substituents. This improved rate for electron-donating substituents is hypothesized to be due to the stabilization of high-oxidation-state intermediates due to the electron density from the ligand, facilitating turnover. The opposite trend—higher activity for complexes bearing electron-withdrawing groups—has been reported for Ir-based WOCs [14], but this has been attributed to the faster activation of Ir precatalysts to give the true active species via the faster loss of electron-deficient ligands. A few studies for Fe and Mn catalysts with systematic ligand variation have helped elucidate the rate-determining step of the mechanism [15] and define the trends in activity and stability for those specific complexes [16].

Systematic studies of ligand modification for Cu WOCs have been challenged by the complete shutdown of catalysis when the ligand changes [17], catalyst degradation under harsh water oxidation conditions, and limitations on the solubility of modified complexes [18]. Comparisons of modified ligands for Cu WOCs have mostly been structural rather than ones that probe electronic effects alone [6,19–21]. A series of complexes bearing modified tetradentate amidate ligands by Llobet and coworkers demonstrated the important role of substituent effects for the single-electron transfer water nucleophilic attack (SET-WNA) mechanism [18]. Incorporating electron-donating substituents (-OMe) enabled the tuning of the overpotential down to a record low of 170 mV at pH 11.5. However, this was accompanied by a corresponding decrease in the rate, as well as loss of faradaic efficiency. A follow-up computational study of the system [22] suggested that the lowered stability might have resulted from a few possible pathways, including hydroxyl attack on the ligand backbone and the greater ease of the protonation of amide groups at a lower pH, leading to ligand dissociation. The electronic properties of the same family of tetra-amidate ligands were further studied by Dey and coworkers, highlighting the ligand-based oxidation steps prior to water oxidation with these redox-active ligands [23].

Our group previously reported a molecular copper water oxidation catalyst bearing the ligand pyalk (2-pyridyl-2-propanate), Cu(pyalk)$_2$ (**1**, Figure 1) [24]. The pyridine anchor combined with the alkoxide moiety has been shown to support high oxidation states, and the gem-dimethyl groups protect the benzylic position from oxidation [25–27]. The simplicity and robustness of the ligand structure led us to investigate the effects of modifying pyalk with electron-donating and electron-withdrawing substituents. In this study, two complexes, Cu(4-MeOOCpyalk)$_2$ (**2**, Figure 1) and Cu(4-MeOpyalk)$_2$ (**3**, Figure 1), were synthesized and analyzed for electrocatalytic WO activity. Both were compared to the previously studied Cu(pyalk)$_2$ to investigate the ligand effects of copper WOCs.
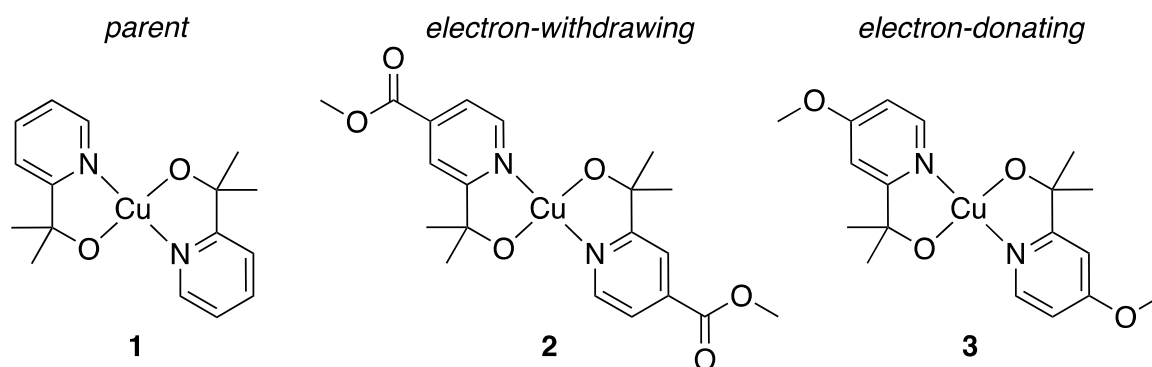

Figure 1. Complexes investigated in this study: the parent complex Cu(pyalk)$_2$ (**1**), Cu(4-MeOOCpyalk)$_2$ (**2**), and Cu(4-MeOpyalk)$_2$ (**3**).

2. Results and Discussion

2.1. Synthesis and Structural Characterization

The ligands 4-MeOOCpyalkH and 4-MeOpyalkH were synthesized using a procedure modified from the literature [28,29], and complexation was accomplished by combining the ligands with $Cu(OAc)_2$ in the presence of KOH (see Section 3). Single crystals of both **2** and **3** were grown via the slow diffusion of pentane into a dichloromethane solution for characterization using X-ray diffraction. The crystals of **2** tended to be small and poorly diffracting, so required the addition of a few drops of pyridine as a co-solvent in order to obtain X-ray-quality crystals. The structures of both **2** and **3** show a bis-ligated, square planar Cu center, with the ligands in a trans orientation (Figure 2). This is consistent with what was previously reported for **1** [24]. The structural parameters (bond distances and angles) of the three complexes are remarkably similar, indicating a well-conserved active site structure (Table 1). Notably, even with the addition of organic substituents, all three complexes were water-soluble, which is advantageous in a homogeneous system designed to oxidize water.
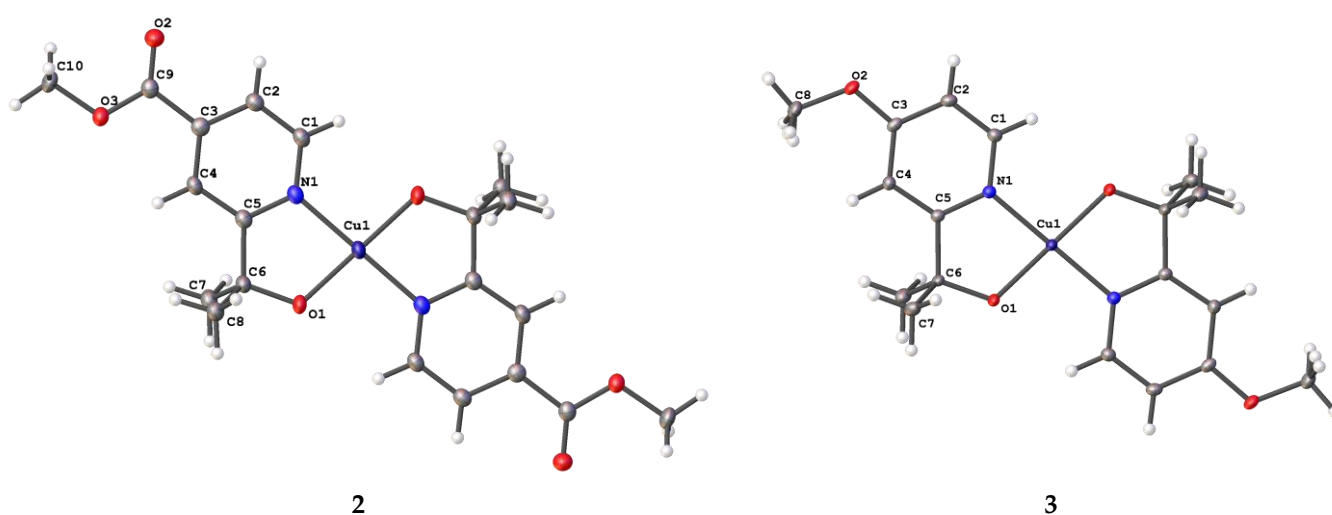

2   **3**

Figure 2. X-ray crystal structures of **2** and **3**. Thermal ellipsoids are shown with 50% probability levels. Hydrogen atoms are shown as circles for clarity, and only the asymmetrical unit is labeled.

Table 1. Selected bond lengths and angles for **1**–**3**.

	1 [1]	**2**	**3**
Cu–N1 (Å)	1.9724 (13)	1.9696 (17)	1.945 (13)
Cu–O1 (Å)	1.8833 (11)	1.8777 (14)	1.8866 (11)
O1–Cu–N1 (°)	84.04 (5)	84.29 (7)	84.33 (5)

[1] From ref. [24].

2.2. pK$_a$ Determination and Comparison

Because of the importance of proton-coupled electron transfer (PCET) in the mechanism of water oxidation [30], as well as the insights gained for electronic tuning, pK_a values were measured for the complexes. The pK_a values of **1**, **2**, and **3** were determined through UV–vis titrations with hydrochloric acid. Clear isosbestic points for all three complexes indicated a clean protonation event. An example titration is shown in Figure 3, and the pK_a values for **1**, **2**, and **3** (an average of at least three titrations) are reported in Table 2. For the data of all of the titrations, see the Supporting Information.
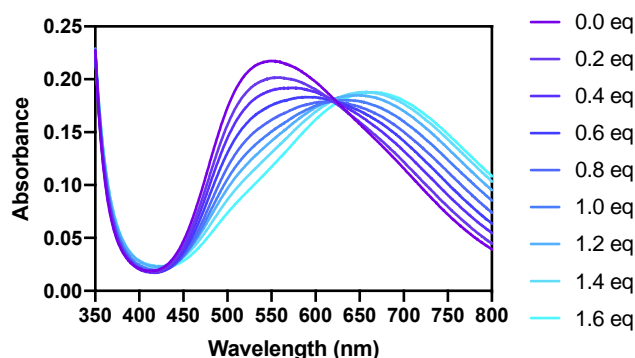
Figure 3. The UV–vis titration of Cu(4-MeOpyalk)$_2$ (**3**) with hydrochloric acid is shown. There is a clear isosbestic point, allowing for the determination of the pK_a.

Table 2. pK_a and λ_{max} values for complexes **1**–**3**, determined via UV–vis spectroscopy.

Complex	pK_a	λ_{max} (nm)
Cu(4-MeOpyalk)$_2$ (**3**)	8.2 ± 0.1	554
Cu(pyalk)$_2$ (**1**)	7.91 ± 0.08	547
Cu(4-MeOOCpyalk)$_2$ (**2**)	7.57 ± 0.08	543

The pK_a is highest for complex **3** at 8.2, as predicted for the electron-donating groups at the para positions. Complex **2** has a lower pK_a (7.57) than **1** (7.91), again in alignment with the expectations from first principles. The shift in the λ_{max} of the UV–vis spectra from 554 to 547 to 543 nm from the electron-donating to electron-withdrawing groups is consistent with the increasing energy of the Cu *d-d* transitions.

2.3. Electrochemical Studies

The electrochemical properties of **2** and **3** were probed using cyclic voltammetry and a boron-doped diamond (BDD) working electrode. At neutral pH, a reversible or quasi-reversible peak was observed for all three complexes upon anodic scanning (Figure 4a). As pyalk has been shown to support high-oxidation-state metal centers without undergoing oxidation itself [24,27,30], this oxidative wave was assigned to a Cu$^{II/III}$ couple and can be used as a measure of electron density at the metal center. A shift in the potential for oxidation was observed, which is in alignment with the expected trends: the electron-donating groups on complex **3** shifted the $E_{1/2}$ less (1.17 V) than the parent complex (1.21 V), while the electron-withdrawing groups on complex **2** shifted the $E_{1/2}$ to a higher potential (1.31 V). $E_{1/2}$ and pK_a were plotted against σ_p Hammett parameters [31] of the ligand para substituents in order to clearly see these trends in Figure S4.

Upon increasing the pH of the electrolyte solution to pH 11 by adding 0.1 M of KOH, an increase in the oxidative current and decrease in reversibility occurs for all three complexes, indicating the onset of water oxidation catalysis (Figure 4b). A similar trend is observed for the catalytic half-peak potential ($E_{p/2}$), as seen for $E_{1/2}$, supporting the proposed mechanism in which the oxidation of Cu^{II} to Cu^{III} initiates catalysis [30]. For homogeneous catalysis, it is common to use $E_{p/2}$ to describe the catalytic potential, although caution must be taken in comparison with other systems that may define this differently [32]. Tuning the electron density around the metal center shifts the $E_{p/2}$, resulting in a difference in overpotential (η) of ~100 mV between complex **2** and complex **3**, where η is defined as the difference between $E_{p/2}$ and the thermodynamic potential for water oxidation at pH 11. As observed in the cyclic voltammetry results in Figure 4b, the peak current for catalysis increases from **3** to **1** to **2**, which could be explained by a rate–overpotential relationship in which higher catalytic activity is expected for catalysts with a higher driving force [33]. The values for $E_{1/2}$, $E_{p/2}$ and η for **1**–**3** are summarized in Table 3.
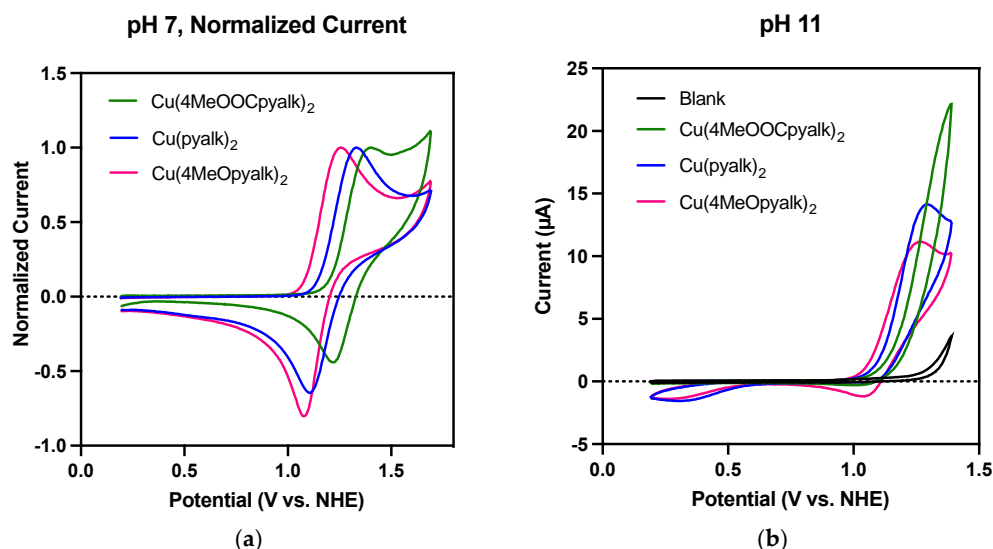
pH 7, Normalized Current (a)

pH 11 (b)

Figure 4. Selected voltammograms for **1**, **2**, and **3**. All were measured using a BDD working electrode, Pt wire counter electrode, and Ag/AgCl reference electrode (sat. KCl, +0.199 V vs. NHE) in 0.1 M KNO$_3$, at a scan rate of 100 mV s^{-1}. (**a**) Non-catalytic CVs were measured at pH 7 and normalized to the peak oxidative current in order to determine $E_{1/2}$ of the reversible or quasi-reversible Cu$^{II/III}$ couples. (**b**) Catalytic waves were measured at pH 11, and the traces were used to determine $E_{p/2}$.

Table 3. $E_{1/2}$, $E_{p/2}$ and η for **1–3**, determined by cyclic voltammetry.

Complex	$E_{1/2}$ (V vs. NHE)	$E_{p/2}$ (V vs. NHE)	η (mV)
Cu(4-MeOpyalk)$_2$ (**3**)	1.17	1.13	550
Cu(pyalk)$_2$ (**1**)	1.21	1.18	600
Cu(4-MeOOCpyalk)$_2$ (**2**)	1.31	1.26	680

2.4. Water Oxidation Activity

To assess the catalytic activity, bulk electrolysis was performed on aqueous solutions of each of the complexes using a fluorine-doped tin oxide (FTO) working electrode with a large surface (~1 cm^2) area, and the oxygen evolution was measured using a Clark-type electrode. The Clark-type electrode was allowed to equilibrate for 1000 s in a basic solution containing the complex, then a potential of 1.2 V vs. NHE was applied to initiate oxygen evolution. Figure 5 compares the detected O$_2$ over time for complexes **1–3**.
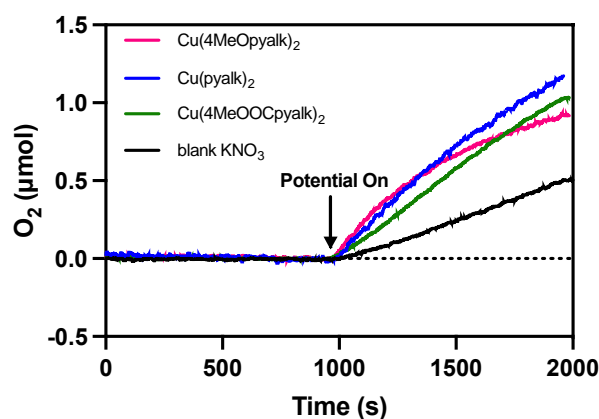

Figure 5. Measurement with a Clark-type electrode shows oxygen evolution upon applying a bias potential. The black line represents the electrolyte solution at pH 11 in the absence of a catalyst, the blue represents the O$_2$ evolution of Cu(pyalk)$_2$, (**1**), in agreement with [24]. The green line represents Cu(4-MeOOCpyalk)$_2$ (**2**), and the pink shows Cu(4-MeOpyalk)$_2$ (**3**).

Cu(pyalk)$_2$ had the highest rate of O$_2$ evolution across the entire 1000 s period of bulk electrolysis (BE). Although **3** had a slightly higher initial rate, the O$_2$ evolution shows a clear decrease over time, signaling the possible decomposition of the complex. Although **2** maintained steady O$_2$ evolution over time, the initial rate was lower than for Cu(pyalk)$_2$. The initial rates were compared because of a lack of stability in **3** over the period of BE. Since the same potential (1.2 V) was applied for all three complexes, these initial rate values are in line with expectations, based on the overpotential and rate relationships [33]. This trend also agrees with the observed increase in $E_{1/2}$ from the electron-donating to -withdrawing substituents. Of note is that the faradaic efficiency (FE) was 90% for **1**, but significantly lower for **2** (79%) and **3** (71%), suggesting the lower robustness of the modified catalysts. The initial rates and FE values are shown in Table 4.

Table 4. Comparison of initial catalytic rate and Faradaic efficiency for complexes **1**–**3**.

Complex	Initial O$_2$ Rate (μmol s^{-1})	Faradaic Efficiency (%)
Cu(4-MeOpyalk)$_2$ (**3**)	0.0020	71
Cu(pyalk)$_2$ (**1**)	0.0019	90
Cu(4-MeOOCpyalk)$_2$ (**2**)	0.0011	79

Initial stability studies were conducted using repeated CV experiments. In total, 100 CV scans were taken for all three complexes using a small-disk BDD electrode (Figure S5). Minimal current drops were observed, with qualitatively more current loss for complexes **2** and **3** than for the parent complex **1**. The BDD electrode was then rinsed, but not polished, and placed in a fresh electrolyte solution. These "rinse tests" showed a minimal current above the blank, suggesting that there is no deposition of catalytically active material on the electrode surface over the 100 CV scans.

To probe the stability of the catalysts over a longer period of time, BE experiments were run with FTO electrodes at 1.2 V vs. NHE for two hours. UV–vis spectra were taken before and after electrolysis to observe what happens to the complexes. Although the current remained remarkably steady over the two hours for all three catalysts (Figure S6), **1** showed only a 5% degradation via UV–vis spectroscopy, while **2** and **3** degraded by 14% and 17%, respectively (Figure S7, Table S1). This is consistent with the faradaic efficiency data, indicating that some amount of charge passed during electrolysis goes to the complex degradation for **2** and **3**, likely ligand oxidation and/or loss. Attempts to characterize ligand oxidation products via NMR spectroscopy were unsuccessful due to the paramagnetic nature of Cu^{2+}, but the oxidative degradation products of pyalk-type ligands have been examined by our group in the past [34]. X-ray photoelectron spectroscopy (XPS) of the FTO electrode surface after a two-hour electrolysis showed a small amount of copper deposition for all three complexes (Figure S8). This suggests that some of the FE loss may go to ligand loss and copper deposition on the electrode. However, the immersion of these electrodes into a fresh electrolyte solution at pH 11 showed minimal catalytic activity via CV and no current at the 1.2 V applied during electrolysis (Figure S9), suggesting that the small amount of copper deposited on the surface is not responsible for the observed homogeneous catalytic activity.

3. Materials and Methods

3.1. Materials and Chemicals

All chemicals were purchased from Sigma-Aldrich or Alfa Aesar and used as received. Complex **1** was synthesized according to procedures reported in the literature [24].

3.2. Synthesis (See Scheme 1)

The *4-MeOOCpyalkH, methyl 2-(2-hydroxypropan-2-yl)isonicotinate* (**L2**) ligand was synthesized following previously reported methods [28].

Cu(4-MeOOCpyalk)$_2$ (**2**). The synthesis of complex **2** was based on previously reported methods [24]. **L2** (50 mg, 0.26 mmol) was added to a solution of copper(II) acetate (24 mg,

0.12 mmol) in 1:9 methanol/acetonitrile (10 mL). The mixture was stirred in air for 30 min and turned a darker blue, then 2.1 equivalents of potassium hydroxide (1 M in methanol) were added and stirred for a further 30 min. The solution turned purple. The solvent was then removed via rotary evaporation, resulting in a purple-brown powder. The solid was redissolved in dichloromethane and filtered through a cotton plug to remove unreacted $Cu(OAc)_2$. Recrystallization via vapor diffusion with pentanes into the CH_2Cl_2 solution with 5 drops of pyridine, which was added as a co-solvent, afforded crystals that were suitable for X-ray diffraction. Isolated yield: 47 mg, 87%. UV/Vis (H_2O): λ_{max} = 543.0 nm. Elemental analysis calculated for $C_{20}H_{24}CuN_2O_6$: C, 53.15; H, 5.35; N, 6.20. Found: C, 52.94; H, 5.34; N, 5.95.

The synthesis of ligand **L3** was based on the methods used to synthesize **L2**.

4-Methoxy-2-acetylpyridine. 4-Methoxypyridine (2.4577 g, 22.5 mmol) and metaldehyde (12.5 g, xs) were dissolved in acetonitrile (90 mL) and stirred at room temperature in air for ten minutes, forming a cloudy white suspension. To this mixture, iron(II) sulfate heptahydrate (0.0909 g, cat.), trifluoroacetic acid (1.34 mL, 17.5 mmol), and 70% tert-butyl hydroperoxide (5.34 mL, 55.5 mmol) were added, forming a cloudy, light-orange suspension. The mixture was put under nitrogen and stirred at reflux for 3.5 h. The mixture changed color from cloudy white to a clear deep red-brown solution. The solution was then cooled to room temperature and the solvent removed via rotary evaporation to leave a red-brown oil. The oil was dissolved in 50 mL of sat. aq. $NaHCO_3$ and was extracted with toluene (5 × 30 mL). The organic layer was dried over Na_2SO_4, filtered, and the solvent was removed via rotary evaporation. The product (1.7953, 51%) was purified via silica gel chromatography using 1:9 ethyl acetate/hexane as the eluent. ^{1}H NMR (400 MHz, $CDCl_3$): δ 8.70 (1H, d), 8.03 (1H, d), 7.87 (1H, dd), 3.80 (3H, s, CH_3), 2.05 (3H, s, CH_3). ESI-MS (m/z): calculated for $C_8H_9NO_2$: 151; found 152, [M+H]+.

4-MeOpyalkH, 2-(4-methoxypyridin-2-yl)propan-2-ol (**L3**). 4-Methoxy-2-acetylpyridine (0.5059 g, 30.1 mmol) was added to a dry Schlenk flask purged with nitrogen. Dry THF (30 mL) was added, forming a clear yellow solution, which was stirred at 0 °C for 30 min. Then, 3.0 M methyl magnesium bromide in diethyl ether (8 mL) was slowly added to the solution. This was stirred at 0 °C for 2.5 h, then warmed to room temperature and stirred for a further 30 min. The reaction was quenched with sat. aq. Ammonium chloride (40 mL), and the solvent was removed via rotary evaporation, resulting in a dark red-brown solid. This solid was dissolved in a 1:1 mixture of sat. aq. Ammonium chloride (50 mL) and ethyl acetate (50 mL), and the product was extracted with dichloromethane (40 mL × 3). The organic layers were dried over $NaSO_4$ for 20 min, filtered, and the solvent removed via rotary evaporation. The resulting product (284.7 mg, 57%) was purified via silica gel chromatography, starting with 1% acetone in dichloromethane, then increasing the eluent concentration to 5% acetone. ^{1}H NMR (400 MHz, $CDCl_3$): δ 8.34 (1H, d), 6.86 (1H, d), 6.72 (1H, dd), 4.99 (1H, s, -OH), 3.87 (3H, s), 1.53 (6H, s). ESI-MS (m/z): calculated for $C_9H_{13}NO_2$: 167; found 168, [M+H]+.

Cu(4-MeOpyalk)$_2$ (**3**). The synthesis of complex **3** was based on previously reported methods [24]. **L3** (50 mg, 0.30 mmol) was added to a solution of copper(II) acetate (27 mg, 0.14 mmol) in 1:9 methanol/acetonitrile (10 mL). The mixture was stirred in air for 30 min and turned a darker blue, then 2.1 equivalents of potassium hydroxide (1 M in methanol) were added, and allowed to stir for a further 30 min, during which the solution turned purple. The solvent was then removed via rotary evaporation, resulting in a purple powder. This solid was redissolved in dichloromethane and filtered through a cotton plug to remove unreacted $Cu(OAc)_2$. Recrystallization via the vapor diffusion of pentanes into the CH_2Cl_2 solution afforded crystals that were suitable for X-ray diffraction. Isolated yield: 50 mg, 90%. UV/Vis (H_2O): λ_{max} = 554.0 nm. Elemental analysis calculated for $C_{18}H_{24}CuN_2O_4$: C, 54.60; H, 6.11; N, 7.08. Found: C, 54.51; H, 6.09; N, 6.91.
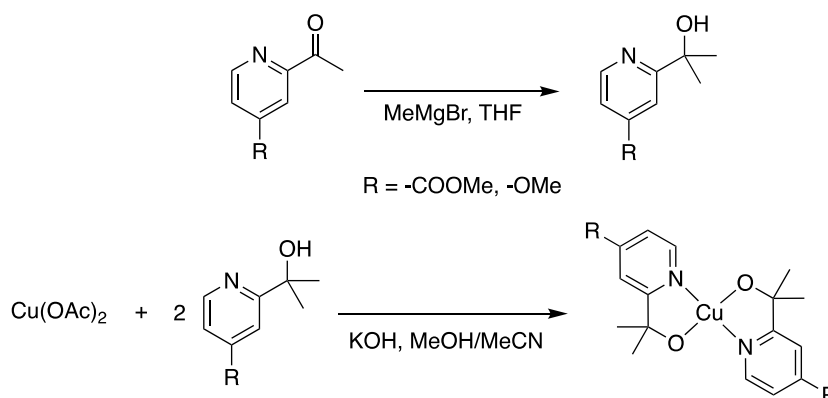
Scheme 1. General synthetic procedure for the synthesis of **L2**, **L3**, **2**, and **3**.

3.3. Instrumentation

^{1}H NMR spectra were recorded on an Agilent DD2 400 MHz spectrometer and chemical shifts were referenced to the residual solvent [δ(CHCl$_3$) = 7.26 ppm]. UV–visible absorption spectra were collected using a Shimadzu UV-2600 UV–vis spectrophotometer. Elemental analyses were performed by Roberson Microlit Laboratories, 1705 US-46 #1d, Ledgewood, NJ 07852. The XPS spectra were collected using a monochromatic 1486.7 eV Al Kα X-ray source on a PHI *VersaProbe* II X-ray Photoelectron Spectrometer with a 0.47 eV system resolution.

Low-temperature X-ray diffraction data (ω-scans) were collected on a Rigaku MicroMax-007HF diffractometer coupled to a Saturn994+ CCD detector with Cu Kα (λ = 1.54178 Å) for the structures of **2** and **3**. The diffraction images of **2** and **3** were processed and scaled using Rigaku Oxford Diffraction software (CrysAlisPro; Rigaku OD: The Woodlands, TX, USA, 2015). All structures were solved with SHELXT and were refined against F2 on all data using full-matrix least squares with SHELXL [35]. All non-hydrogen atoms were refined anisotropically. Hydrogen atoms were included in the model at geometrically calculated positions and refined using a riding model. The isotropic displacement parameters of all hydrogen atoms were fixed to 1.2 times the U value of the atoms to which they are linked (1.5 times for methyl groups). The only exceptions are the protons associated with C8 for **3**, which were added as a disordered group at 0.5 occupancy. The data for **2** were refined as a two-component twin. The fractional volume contribution of the minor twin component was freely refined to a converged value of 0.5146(14). A summary of the crystal data and structure refinement can be found in the Supporting Information (Table S2).

3.4. Electrochemical Measurements

Cyclic voltammetry measurements were made using a Pine Wavenow potentiostat or a CHI 660E potentiostat. The three-electrode set-up included a 3 mm diameter boron-doped diamond (BDD) working electrode, a Pt wire counter electrode, and a Ag/AgCl (sat. KCl) reference electrode (0.199 V vs. NHE). CVs were collected at a 100 mV/s scan rate.

O$_2$ evolution measurements were performed in an air-tight electrochemical cell containing 1 mM of complex in 0.1 M of KNO$_3$ electrolyte adjusted to the appropriate pH value with 0.1 M of KOH. The electrodes used were a 1 cm^2 fluorine-doped tin oxide (FTO) working electrode, an Ag/AgCl (saturated with KCl) reference electrode, and a Pt counter electrode. The cell was fitted with a Clark-type electrode for O$_2$ detection. The air-saturated O$_2$ concentration in water was calculated prior to catalytic measurements and was used to calculate baseline readings. During electrochemical O$_2$ assays, no applied bias was taken during the first 1000 s of each experiment to obtain a baseline reading. After the baseline reading, a bias of 1.2 V vs. NHE was applied to the electrochemical cell to initiate water oxidation catalysis.

4. Conclusions

In conclusion, two new complexes were synthesized to examine the effects of ligand tuning on the electrocatalytic water oxidation activity of the reported Cu(pyalk)$_2$ complex. The trends in pK_a and the redox potential align with first-principles predictions for the electron-withdrawing and electron-donating groups. The electron-donating methoxy groups led to a higher pK_a and a lower potential for oxidation, while the electron-withdrawing carboxymethyl groups corresponded to a lower pK_a and a higher potential for oxidation. O$_2$ evolution experiments revealed a consistent trend with these data. The methoxy derivative was initially a faster catalyst but soon deactivated, plausibly by oxidative degradation at the methoxy group, emphasizing the cardinal importance of oxidative robustness in ligand design for WOCs. The carboxymethyl derivative was slower but more robust, leaving the original catalyst with the best compromise between activity and robustness.

This study is one of only a few systematic studies of ligand modification for Cu WOCs bearing oxidation-resistant ligands, and has increased our understanding of the catalysis of water oxidation and how it is affected by ligand electronic effects. For first-row transition metals to be useful in an artificial photosynthetic system, further work is needed to sidestep the rate–overpotential scaling relationship to develop catalysts with a lower overpotential and an increased rate that have long-term stability and operate under relevant conditions. Since an ultimate goal in the field is to attach molecular catalysts onto semiconductor surfaces for an operable photoanode, the insights gained from ligand modification studies such as this one can help to highlight important synthetic considerations for catalyst anchoring.

References

1. Lewis, N.S.; Nocera, D.G. Powering the Planet: Chemical Challenges in Solar Energy Utilization. *Proc. Natl. Acad. Sci. USA* **2006**, *103*, 15729–15735. [CrossRef]
2. Zhang, B.; Sun, L. Artificial Photosynthesis: Opportunities and Challenges of Molecular Catalysts. *Chem. Soc. Rev.* **2019**, *48*, 2216–2264. [CrossRef]
3. Blakemore, J.D.; Crabtree, R.H.; Brudvig, G.W. Molecular Catalysts for Water Oxidation. *Chem. Rev.* **2015**, *115*, 12974–13005. [CrossRef]
4. Barnett, S.M.; Goldberg, K.I.; Mayer, J.M. A Soluble Copper–Bipyridine Water-Oxidation Electrocatalyst. *Nat. Chem.* **2012**, *4*, 498–502. [CrossRef]

5. Lee, H.; Wu, X.; Sun, L. Copper-Based Homogeneous and Heterogeneous Catalysts for Electrochemical Water Oxidation. *Nanoscale* **2020**, *12*, 4187–4218. [CrossRef]

6. Chen, Q.-F.; Cheng, Z.-Y.; Liao, R.-Z.; Zhang, M.-T. Bioinspired Trinuclear Copper Catalyst for Water Oxidation with a Turnover Frequency up to 20000 s^{-1}. *J. Am. Chem. Soc.* **2021**, *143*, 19761–19768. [CrossRef]

7. Yu, K.; Sun, Y.; Zhu, D.; Xu, Z.; Wang, J.; Shen, J.; Zhang, Q.; Zhao, W. A Low-Cost Commercial Cu(ii)–EDTA Complex for Electrocatalytic Water Oxidation in Neutral Aqueous Solution. *Chem. Commun.* **2022**, *58*, 12835–12838. [CrossRef]

8. Wu, X.; Li, F.; Zhang, B.; Sun, L. Molecular Complexes in Water Oxidation: Pre-Catalysts or Real Catalysts. *J. Photochem. Photobiol. C Photochem. Rev.* **2015**, *25*, 71–89. [CrossRef]

9. Gil-Sepulcre, M.; Llobet, A. Molecular Water Oxidation Catalysts Based on First-Row Transition Metal Complexes. *Nat. Catal.* **2022**, *5*, 79–82. [CrossRef]

10. Wasylenko, D.J.; Ganesamoorthy, C.; Koivisto, B.D.; Henderson, M.A.; Berlinguette, C.P. Insight into Water Oxidation by Mononuclear Polypyridyl Ru Catalysts. *Inorg. Chem.* **2010**, *49*, 2202–2209. [CrossRef]

11. Maji, S.; López, I.; Bozoglian, F.; Benet-Buchholz, J.; Llobet, A. Mononuclear Ruthenium–Water Oxidation Catalysts: Discerning between Electronic and Hydrogen-Bonding Effects. *Inorg. Chem.* **2013**, *52*, 3591–3593. [CrossRef]

12. Abdel-Magied, A.F.; Arafa, W.A.A.; Laine, T.M.; Shatskiy, A.; Kärkäs, M.D.; Åkermark, B.; Johnston, E.V. Substituent Effects in Molecular Ruthenium Water Oxidation Catalysts Based on Amide Ligands. *Chemcatchem* **2017**, *9*, 1583–1587. [CrossRef]

13. Watabe, S.; Tanahashi, Y.; Hirahara, M.; Yamazaki, H.; Takahashi, K.; Mohamed, E.A.; Tsubonouchi, Y.; Zahran, Z.N.; Saito, K.; Yui, T.; et al. Critical Hammett Electron-Donating Ability of Substituent Groups for Efficient Water Oxidation Catalysis by Mononuclear Ruthenium Aquo Complexes. *Inorg. Chem.* **2019**, *58*, 12716–12723. [CrossRef]

14. Rodriguez, G.M.; Zaccaria, F.; Van Dijk, S.; Zuccaccia, C.; Macchioni, A. Substituent Effects on the Activity of Cp*Ir(Pyridine-Carboxylate) Water Oxidation Catalysts: Which Ligand Fragments Remain Coordinated to the Active Ir Centers? *Organometallics* **2021**, *40*, 3445–3453. [CrossRef]

15. Codolà, Z.; Garcia-Bosch, I.; Acuña-Parés, F.; Prat, I.; Luis, J.M.; Costas, M.; Lloret-Fillol, J. Electronic Effects on Single-Site Iron Catalysts for Water Oxidation. *Chem. A Eur. J.* **2013**, *19*, 8042–8047. [CrossRef]

16. Rohner, S.S.; Kinzel, N.W.; Werlé, C.; Leitner, W. Systematic Ligand Variation to Modulate the Electrochemical Properties of Iron and Manganese Complexes. *Dalton Trans.* **2019**, *48*, 13205–13211. [CrossRef]

17. Gerlach, D.L.; Bhagan, S.; Cruce, A.A.; Burks, D.B.; Nieto, I.; Truong, H.T.; Kelley, S.P.; Herbst-Gervasoni, C.J.; Jernigan, K.L.; Bowman, M.K.; et al. Studies of the Pathways Open to Copper Water Oxidation Catalysts Containing Proximal Hydroxy Groups during Basic Electrocatalysis. *Inorg. Chem.* **2014**, *53*, 12689–12698. [CrossRef]

18. Garrido-Barros, P.; Funes-Ardoiz, I.; Drouet, S.; Benet-Buchholz, J.; Maseras, F.; Llobet, A. Redox Non-Innocent Ligand Controls Water Oxidation Overpotential in a New Family of Mononuclear Cu-Based Efficient Catalysts. *J. Am. Chem. Soc.* **2015**, *137*, 6758–6761. [CrossRef]

19. Shen, J.; Zhang, X.; Cheng, M.; Jiang, J.; Wang, M. Electrochemical Water Oxidation Catalyzed by N$_4$-Coordinate Copper Complexes with Different Backbones: Insight into the Structure-Activity Relationship of Copper Catalysts. *Chemcatchem* **2020**, *12*, 1302–1306. [CrossRef]

20. Shen, J.; Wang, M.; Gao, J.; Han, H.; Liu, H.; Sun, L. Improvement of Electrochemical Water Oxidation by Fine-Tuning the Structure of Tetradentate N$_4$ Ligands of Molecular Copper Catalysts. *Chemsuschem* **2017**, *10*, 4581–4588. [CrossRef]

21. Garrido-Barros, P.; Moonshiram, D.; Gil-Sepulcre, M.; Pelosin, P.; Gimbert-Suriñach, C.; Benet-Buchholz, J.; Llobet, A. Redox Metal–Ligand Cooperativity Enables Robust and Efficient Water Oxidation Catalysis at Neutral pH with Macrocyclic Copper Complexes. *J. Am. Chem. Soc.* **2020**, *142*, 17434–17446. [CrossRef]

22. de Aguirre, A.; Garrido-Barros, P.; Funes-Ardoiz, I.; Maseras, F. The Role of Electron-Donor Substituents in the Family of OPBAN-Cu Water Oxidation Catalysts: Effect on the Degradation Pathways and Efficiency. *Eur. J. Inorg. Chem.* **2019**, *2019*, 2109–2114. [CrossRef]

23. Chattopadhyay, S.; Ghatak, A.; Ro, Y.; Guillot, R.; Halime, Z.; Aukauloo, A.; Dey, A. Ligand Radical Mediated Water Oxidation by a Family of Copper *o*-Phenylene Bis-Oxamidate Complexes. *Inorg. Chem.* **2021**, *60*, 9442–9455. [CrossRef]

24. Fisher, K.J.; Materna, K.L.; Mercado, B.Q.; Crabtree, R.H.; Brudvig, G.W. Electrocatalytic Water Oxidation by a Copper(II) Complex of an Oxidation-Resistant Ligand. *ACS Catal.* **2017**, *7*, 3384–3387. [CrossRef]

25. Michaelos, T.K.; Shopov, D.Y.; Sinha, S.B.; Sharninghausen, L.S.; Fisher, K.J.; Lant, H.M.C.; Crabtree, R.H.; Brudvig, G.W. A Pyridine Alkoxide Chelate Ligand That Promotes both Unusually High Oxidation States and Water-Oxidation Catalysis. *Acc. Chem. Res.* **2017**, *50*, 952–959. [CrossRef]

26. Shopov, D.Y.; Sharninghausen, L.S.; Sinha, S.B.; Mercado, B.Q.; Balcells, D.; Brudvig, G.W.; Crabtree, R.H. A Dinuclear Iridium(V,V) Oxo-Bridged Complex Characterized Using a Bulk Electrolysis Technique for Crystallizing Highly Oxidizing Compounds. *Inorg. Chem.* **2018**, *57*, 5684–5691. [CrossRef]

27. Fisher, K.J.; Feuer, M.L.; Lant, H.M.C.; Mercado, B.Q.; Crabtree, R.H.; Brudvig, G.W. Concerted Proton-Electron Transfer Oxidation of Phenols and Hydrocarbons by a High-Valent Nickel Complex. *Chem. Sci.* **2020**, *11*, 1683–1690. [CrossRef]

28. Materna, K.L.; Rudshteyn, B.; Brennan, B.J.; Kane, M.H.; Bloomfield, A.J.; Huang, D.L.; Shopov, D.Y.; Batista, V.S.; Crabtree, R.H.; Brudvig, G.W. Heterogenized Iridium Water-Oxidation Catalyst from a Silatrane Precursor. *ACS Catal.* **2016**, *6*, 5371–5377. [CrossRef]

29. Wong, Y.-L.; Yang, Q.; Zhou, Z.-Y.; Lee, H.K.; Mak, T.C.W.; Ng, D.K.P. Synthesis, Structure and Oxo-Transfer Properties of Dioxotungsten(VI) Complexes with Pyridine-Based NO-and NS-Bidentate Ligands. *New J. Chem.* **2001**, *25*, 353–357. [CrossRef]

30. Rudshteyn, B.; Fisher, K.J.; Lant, H.M.C.; Yang, K.R.; Mercado, B.Q.; Brudvig, G.W.; Crabtree, R.H.; Batista, V.S. Water-Nucleophilic Attack Mechanism for the $Cu^{II}(Pyalk)_2$ Water-Oxidation Catalyst. *ACS Catal.* **2018**, *8*, 7952–7960. [CrossRef]

31. Hansch, C.; Leo, A.; Taft, R.W. A Survey of Hammett Substituent Constants and Resonance and Field Parameters. *Chem. Rev.* **1991**, *91*, 165–195. [CrossRef]

32. Rountree, E.S.; McCarthy, B.D.; Eisenhart, T.T.; Dempsey, J.L. Evaluation of Homogeneous Electrocatalysts by Cyclic Voltammetry. *Inorg. Chem.* **2014**, *53*, 9983–10002. [CrossRef] [PubMed]

33. Costentin, C.; Drouet, S.; Robert, M.; Savéant, J.-M. Turnover Numbers, Turnover Frequencies, and Overpotential in Molecular Catalysis of Electrochemical Reactions. Cyclic Voltammetry and Preparative-Scale Electrolysis. *J. Am. Chem. Soc.* **2012**, *134*, 11235–11242. [CrossRef]

34. Shopov, D.Y.; Sharninghausen, L.S.; Sinha, S.B.; Mercado, B.Q.; Brudvig, G.W.; Crabtree, R.H. Modification of a Pyridine-Alkoxide Ligand during the Synthesis of Coordination Compounds. *Inorganica Chim. Acta* **2019**, *484*, 75–78. [CrossRef]

35. Sheldrick, G.M. A Short History of SHELX. *Acta Crystallogr. Sect. A Found. Crystallogr.* **2008**, *64*, 112–122. [CrossRef] [PubMed]